The Solid State Forms of the Sex Hormone 17-β-Estradiol

Erin L. Stevenson, Robert W. Lancaster, Asma B. M. Buanz, Louise S. Price, Derek A. Tocher, Sarah L. Price

Electronic Supporting Information

Table of Contents

A) Experimental

Section 1   Solid Form Screening Experiments

1.1.   Slow Evaporative Crystallization.

The hemihydrate crystals (BES·0.5H$_2$O) were produced by dissolving microcrystalline BES·0.5H$_2$O in analytical grade solvents and left to evaporate at either room temperature (~25 °C) or in a refrigerator for even slower evaporation (~5 °C). Crystallization took approximately 5 days.

The methanol hemisolvate crystals (BES·0.5MeOH) were produced by dissolving microcrystalline BES·0.5H$_2$O in analytical grade methanol. Crystals were produced when the solution was left to slowly evaporate at RT or at 5 °C with the lid left on the sample vial for approximately 2 weeks.

Table S 1. Summary of slow evaporative crystallization methods in which BES·0.5H$_2$O and BES·0.5MeOH were produced. All samples in this case were left to evaporate in air.

Solvent Used	Concentration in 3 mL (g mL^{-1})	RT Lid Left On Sample Vial	RT Lid Left Off Sample Vial	5°C Lid Left On Sample Vial	5°C Lid Left Off Sample Vial
ethanol	0.0033	♦	♦	♦	♦
	0.0016	♦	♦	♦	♦
acetonitrile	0.0033	♦	♦	♦	♦
	0.0016	♦	♦	♦	♦
ethyl acetate	0.0033	♦	♦	♦	♦
	0.0016	♦	♦	♦	♦
diethyl ether	0.0033	○	○	○	○
	0.0016	○	○	♦	○
acetone	0.0033	○	○	○	○
	0.0016	○	○	○	○
isopropanol	0.0033	♦	♦	○	○
	0.0016	○	○	○	○
n-butanol	0.0033	♦	♦	○	○
	0.0016	○	○	○	○
isopropyl ether	0.0033	○	♦	○	○
	0.0016	○	○	○	○
n-butyl ether	0.0033	○	♦	○	○
	0.0016	○	○	○	○
methanol	0.0033	●	○	●	○
	0.0016	●	○	●	○

♦ Single crystals of BES·0.5H$_2$O. IR spectrum identical to starting material.

○ No single crystals produced, IR spectrum identical to starting material and BES·0.5H$_2$O .

●Single crystals of BES·MeOH

Slow evaporative techniques from dry solvents were used to produce alternative solvate forms. These solvents were obtained as anhydrous and stored over molecular sieves (size 3 Å). The solutions were left to evaporate in small sample vials with the lids left off, in a P$_2$O$_5$ filled desiccator to maintain a dry environment for crystallization. Crystals of BES·PrOH, BES·ACN and BES Form I took approximately 2 – 3 weeks to grow. Crystals of BES·EDC took approximately 2 months to grow.

Table S 2. Summary of slow evaporative crystallization methods with anhydrous solvents.

Solvent Used	Concentration	Solid Form Produced	Data Collection
ethylene dichloride	0.0033	BES·EDC	X ▲ ● *
	0.0016	BES·EDC	-
n-propanol	0.0033	BES·PrOH	♦ ▲ ● *
	0.0016	BES·PrOH	-
acetonitrile	0.0033	BES·ACN	♦ ▲ ● *
	0.0016	BES·ACN	-
n-butanol	0.0033	Crystals not grown	-
	0.0016	Crystals not grown	-
ethyl acetate	0.0033	BES.anhyd2	*
	0.0016	BES.anhyd2	*
diethyl ether	0.0033	BES.anhyd2	*
	0.0016	BES.anhyd2	*

♦ Single crystals obtained and SCXRD data collected, X the data completion is only 82% from best crystals obtained.

● PXRD data collected

▲ DSC and TGA data collected

* IR data collected, BES.anhyd2 is an unidentified form that may correspond to the elusive Form II

- Insufficient material for analysis

There was insufficient material for DSC, TGA and PXRD analysis of BES·PrOH and BES·EDC and for PXRD analysis of BES·0.5MeOH and BES·ACN due to low yields and difficulty in reproducing these forms in competition with BES·0.5H$_2$O.

1.2. Evaporation to Dryness from Boiling Solution Crystallization

Anhydrous BES Form I was produced by dissolving 17-β-estradiol hemihydrate (~0.01g) in ethyl acetate (~6 mL) and heating the solution on a hot plate until the solution was evaporated to dryness. This gave BES Form I as a white microcrystalline powder.

1.3. Cooling Crystallizations

Cooling crystallization experiments were performed by placing microcrystalline BES·0.5H$_2$O (~0.01g) in an oven at a certain temperature (see Table S 3), holding the samples at that temperature for a period of time and subsequent cooling at varied rates. A summary of all cooling crystallization experiments performed and their outcomes is presented in Table S 3.

Table S 3. Summary of cooling crystallization methods.

Temperature at which the sample was left (°C)	Period of time left at temperature (h)	Cooling rate (°C min^{-1})	Solid form produced
150	4	1	BES Form I
	4	uncontrolled	BES Form I
178	1	1	BES Form I
	1	uncontrolled	BES Form I
	2	1	BES$_{(am)}$
	2	uncontrolled	BES$_{(am)}$
185	1	1	BES Form I
	1	uncontrolled	BES$_{(am)}$
	2	1	BES$_{(am)}$
	2	uncontrolled	BES Form I

In the instances when the cooling process was uncontrolled, the oven was turned off and the material was left in the oven until RT was reached. All samples were then stored in a P_2O_5 desiccator.

1.4. Sublimation Crystallizations

Microcrystalline BES Form I was produced from heating the hemihydrate starting material in an oven to 150 °C for 4 hours and subsequently cooling to room temperature. Sublimation experiments were performed by sealing a small amount of microcrystalline BES Form I (~100mg) in Pyrex tubing at approximately 5×10^{-2} mmHg and heating in a tube furnace with a temperature gradient from 150 °C to RT. Crystals were produced after 1 week.

Section 2   Infrared Spectra

2.1. Hemihydrate (BES·0.5H₂O)
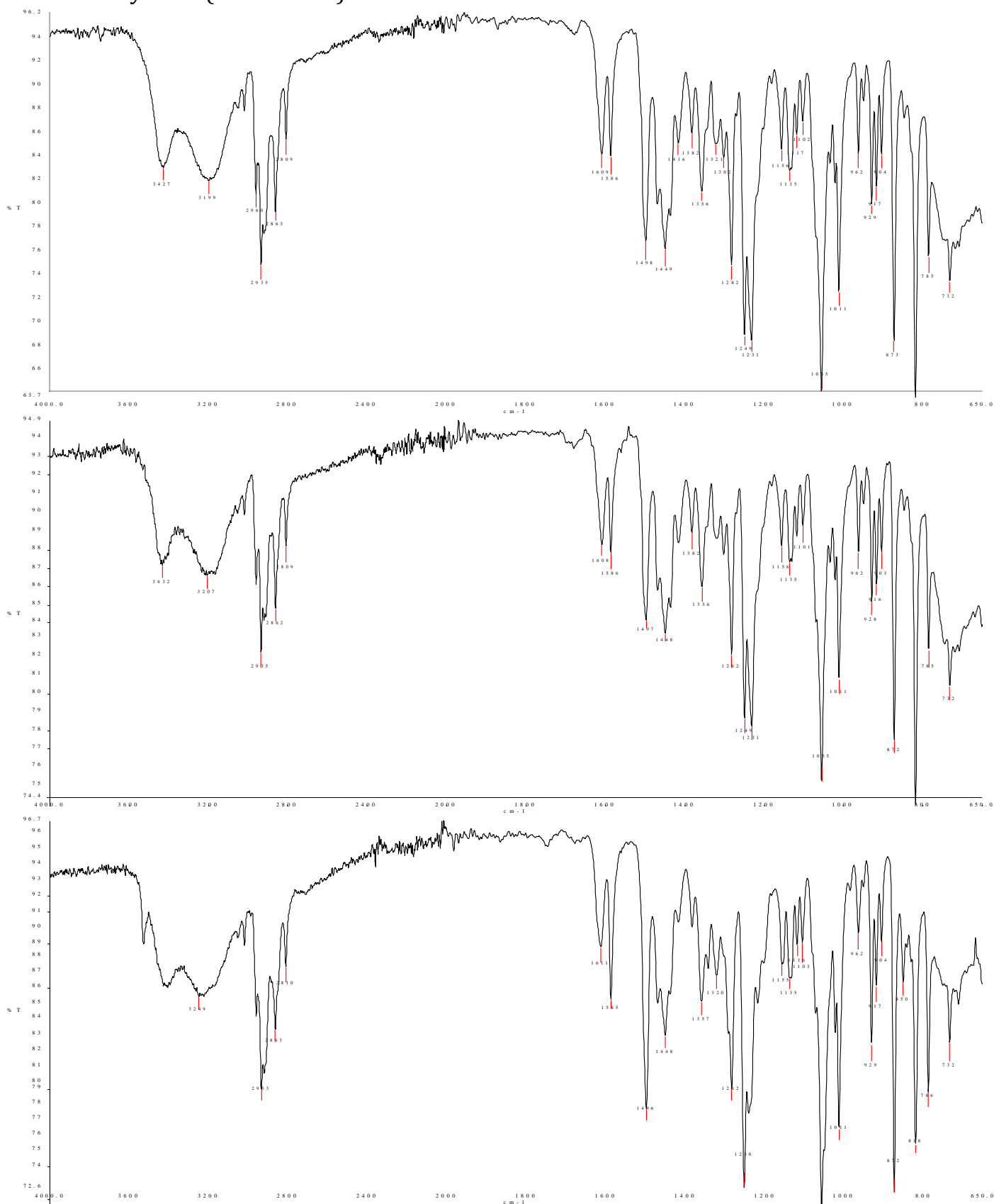
Figure S 1. 17-β-estradiol hemihydrate (top) starting material, (middle) crystallized from solvents included in Table S 1, and (bottom) left in a P₂O₅ desiccator for 6 weeks. The peak at 3600 cm⁻¹ for material kept in the desiccator (bottom) may indicate some rearrangement to give some OH groups that are not involved in hydrogen bonding, probably due to a small degree of dehydration.

5

2.2. Solvates of 17-β-estradiol
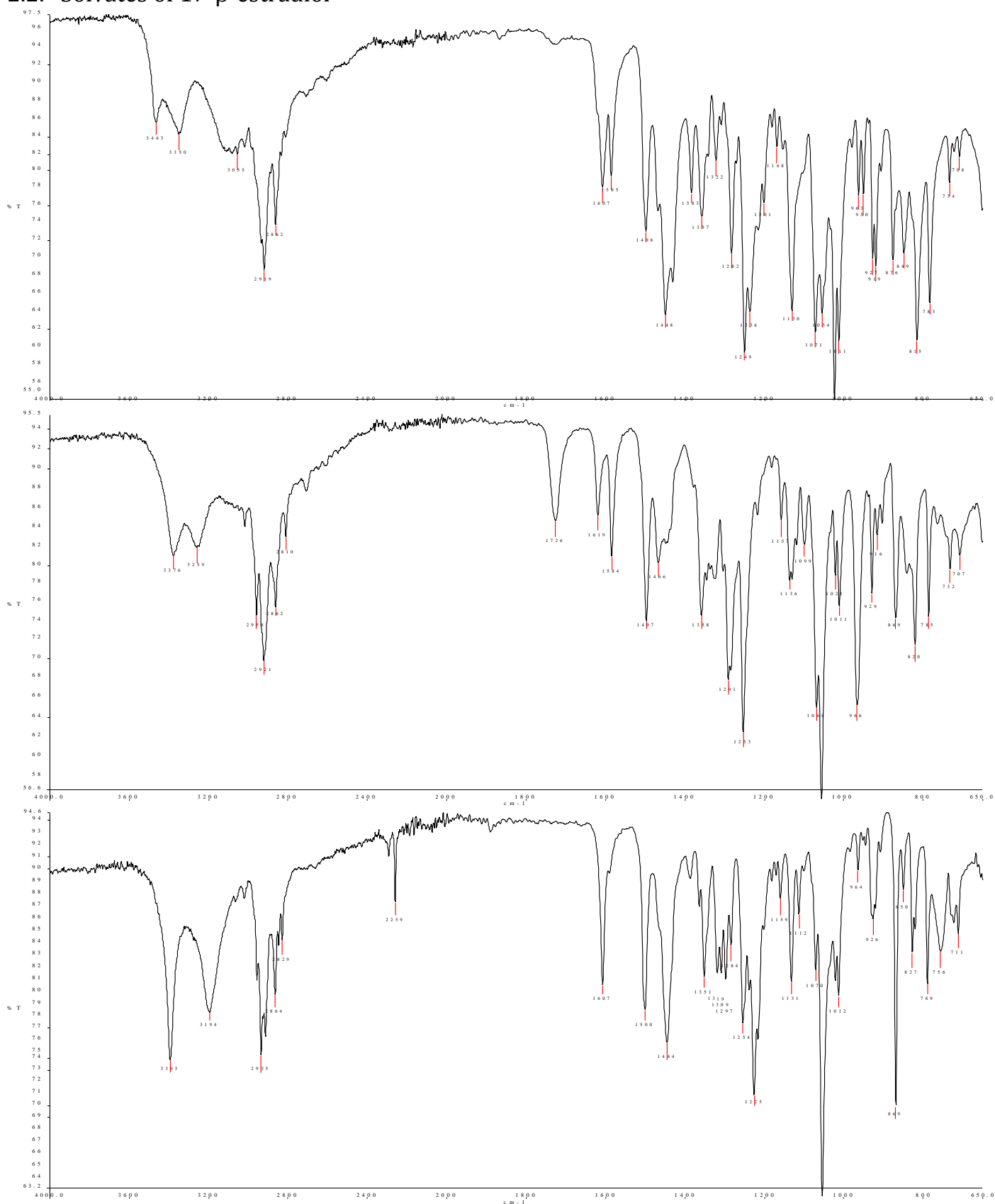
Figure S 2. *(top) BES·0.5MeOH crystallized from analytical grade methanol, crystallization conditions in Table S 1, (middle) BES·PrOH crystallized from anhydrous n-propanol, crystallization conditions in Table S 2 (the additional peak at 1726 cm^{-1} may be due to the presence of some keto form), and (bottom) BES·ACN, crystallization conditions in Table S 2 with the solvent CN vibration at 2259 cm^{-1}.*

2.3. Anhydrous Forms.
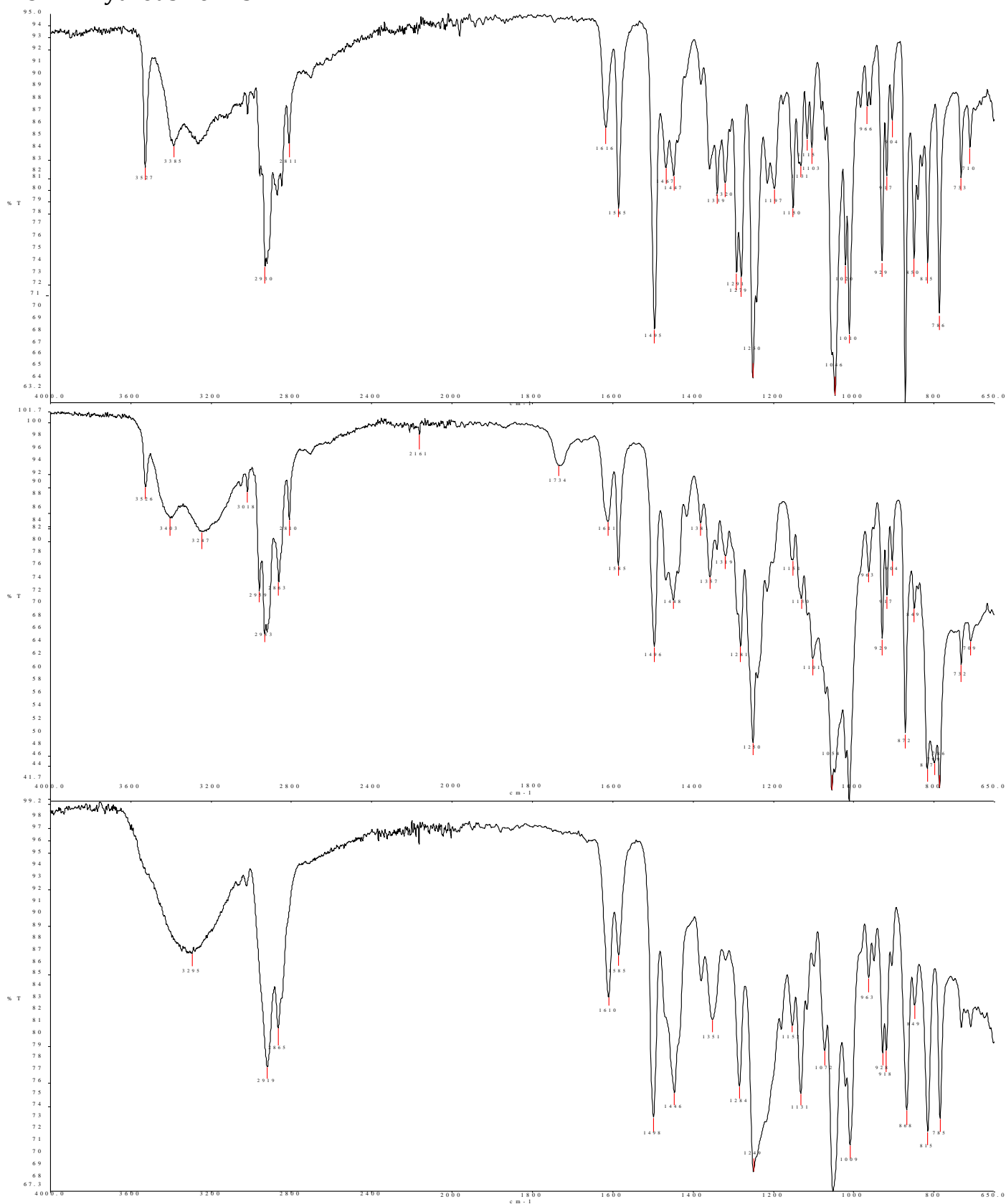
Figure S 3. (top) BES Form I (crystallization conditions in section 1; the peak at 3527 cm^{-1} is the OH group not involved in hydrogen bonding), (middle) BES.anhyd2 obtained by slow crystallization from e.g. anhydrous ethyl acetate (Table S 2; this contains the peaks of Form I and also the ketone peak at 1734 cm^{-1}, possibly from form II), and (bottom) BES$_{(am)}$ conditions in section 1.

Section 3 Crystallographic Data

3.1. SCXRD Data

Table S 4. Crystallographic data.

Phase Designator	BES·0.5H$_2$O	BES·0.5MeOH	BES·PrOH	BES·ACN	BES Form I
Empirical formula	C$_{18}$H$_{25}$O$_{2.5}$	C$_{37}$H$_{52}$O$_5$	C$_{21}$H$_{32}$O$_3$	C$_{20}$H$_{27}$NO$_2$	C$_{36}$H$_{48}$O$_4$
Formula weight	281.38	576.78	332.46	313.42	544.74
Temperature/K	150.00(10)	150(1)	149.98(10)	160.00(10)	150.00(10)
Crystal system	orthorhombic	triclinic	orthorhombic	orthorhombic	orthorhombic
Space group	P22$_1$2$_1$	P1	P2$_1$2$_1$2$_1$	P2$_1$2$_1$2$_1$	P2$_1$2$_1$2$_1$
a/Å	6.54127(8)	7.31144(16)	6.58547(6)	6.98287(7)	6.41117(7)
b/Å	12.05549(14)	9.2985(2)	23.9331(3)	13.56289(14)	12.19725(13)
c/Å	19.2527(2)	12.3778(2)	12.23603(11)	18.1895(2)	37.9575(4)
α/°	90	89.7413(17)	90	90	90
β/°	90	88.0129(17)	90	90	90
γ/°	90	70.786(2)	90	90	90
Volume/Å^3	1518.23(3)	794.14(3)	1928.53(3)	1722.69(3)	2968.23(6)
Z	4	2	4	4	4
ρ_{calc}/g cm^{-3}	1.231	1.206	1.145	1.208	1.219
μ/mm^{-1}	0.631	0.615	0.585	0.603	0.604
F(000)	612.0	314.0	728.0	680.0	1184.0
Crystal size/mm^3	0.3 × 0.3 × 0.3	0.4 × 0.3 × 0.3	0.4 × 0.2 × 0.1	0.5 × 0.1 × 0.1	0.3 × 0.2 × 0.1
Radiation	CuKα (λ = 1.54184)	CuKα (λ = 1.54184)	CuKα (λ = 1.54184)	CuKα (λ = 1.54184)	CuKα (λ = 1.54184)
2Θ range for data collection/°	11.764 to 147.086	10.074 to 147.19	7.388 to 147.28	8.132 to 147.392	7.614 to 147.422
Index ranges	-8 ≤ h ≤ 7 -14 ≤ k ≤ 14 -22 ≤ l ≤ 23	-8 ≤ h ≤ 8 -11 ≤ k ≤ 11 -15 ≤ l ≤ 15	-8 ≤ h ≤ 8 -29 ≤ k ≤ 28 -14 ≤ l ≤ 15	-8 ≤ h ≤ 8 -16 ≤ k ≤ 16 -22 ≤ l ≤ 22	-7 ≤ h ≤ 7 -15 ≤ k ≤ 15 -47 ≤ l ≤ 47
Reflections collected	5285	11899	29872	25514	48838
Independent reflections	2945 [R_{int} = 0.0171, R_{sigma} = 0.0209]	5763 [R_{int} = 0.0146, R_{sigma} = 0.0119]	3880 [R_{int} = 0.0422, R_{sigma} = 0.0171]	3456 [R_{int} = 0.0444, R_{sigma} = 0.0187]	5932 [R_{int} = 0.0520, R_{sigma} = 0.0222]
Data/restraints/parameters	2945/0/280	5763/3/587	3880/0/225	3456/0/316	5932/0/417
Goodness-of-fit on F^2	1.047	1.052	1.030	1.050	1.073
Final R indexes [I>=2σ (I)]	R_1 = 0.0369, wR_2 = 0.0992	R_1 = 0.0254, wR_2 = 0.0739	R_1 = 0.0357, wR_2 = 0.0975	R_1 = 0.0358, wR_2 = 0.0938	R_1 = 0.0384, wR_2 = 0.1003
Final R indexes [all data]	R_1 = 0.0371, wR_2 = 0.0995	R_1 = 0.0254, wR_2 = 0.0739	R_1 = 0.0366, wR_2 = 0.0989	R_1 = 0.0369, wR_2 = 0.0956	R_1 = 0.0397, wR_2 = 0.1015
Largest diff. peak/hole / e Å^{-3}	0.26/-0.18	0.20/-0.12	0.19/-0.20	0.19/-0.18	0.20/-0.20
Flack parameter	-0.03(7)	0.08(4)	-0.07(6)	0.09(8)	-0.07(7)
CCDC deposition number	CCDC 1875325	CCDC 1875323	CCDC 1875326	CCDC 1875324	CCDC 1875327

3.2. PXRD Data
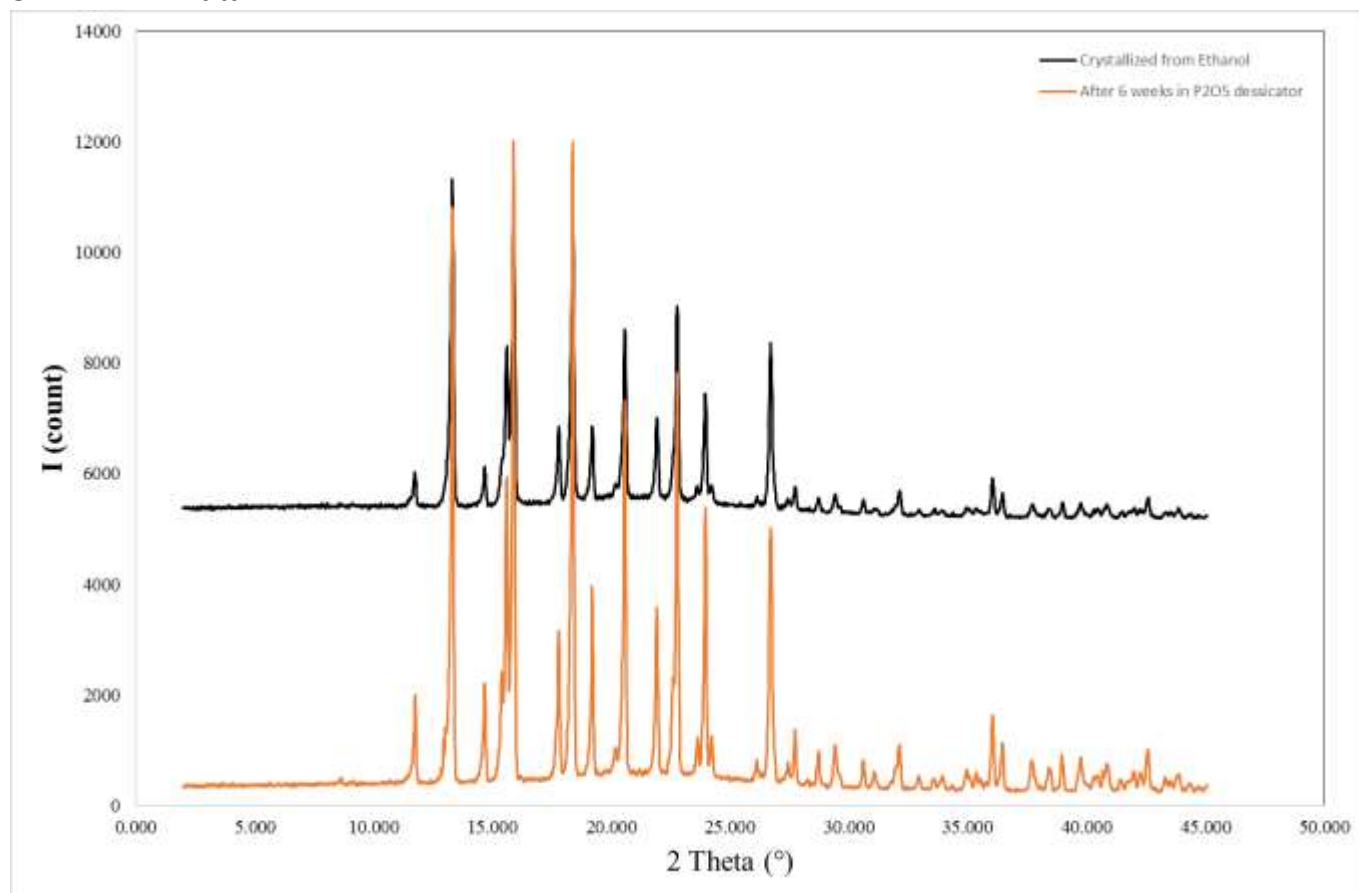
Figure S 4. PXRD pattern for BES·0.5H$_2$O crystallized from ethanol (black; 5.0 s per step) and after 6 weeks in a P$_2$O$_5$-filled desiccator (orange).
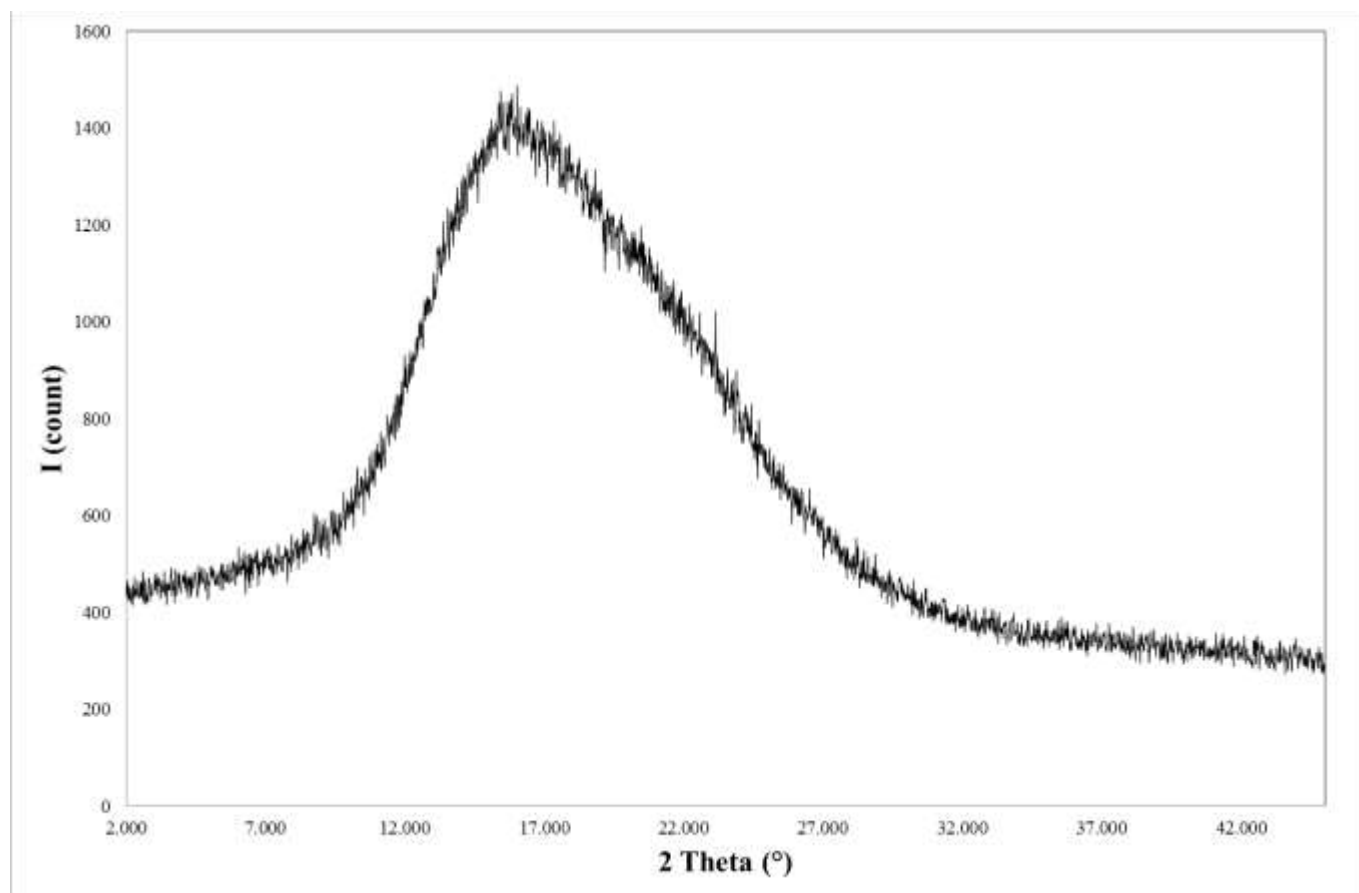
Figure S 5. PXRD data of BES$_{(am)}$ confirming the amorphous character.

9
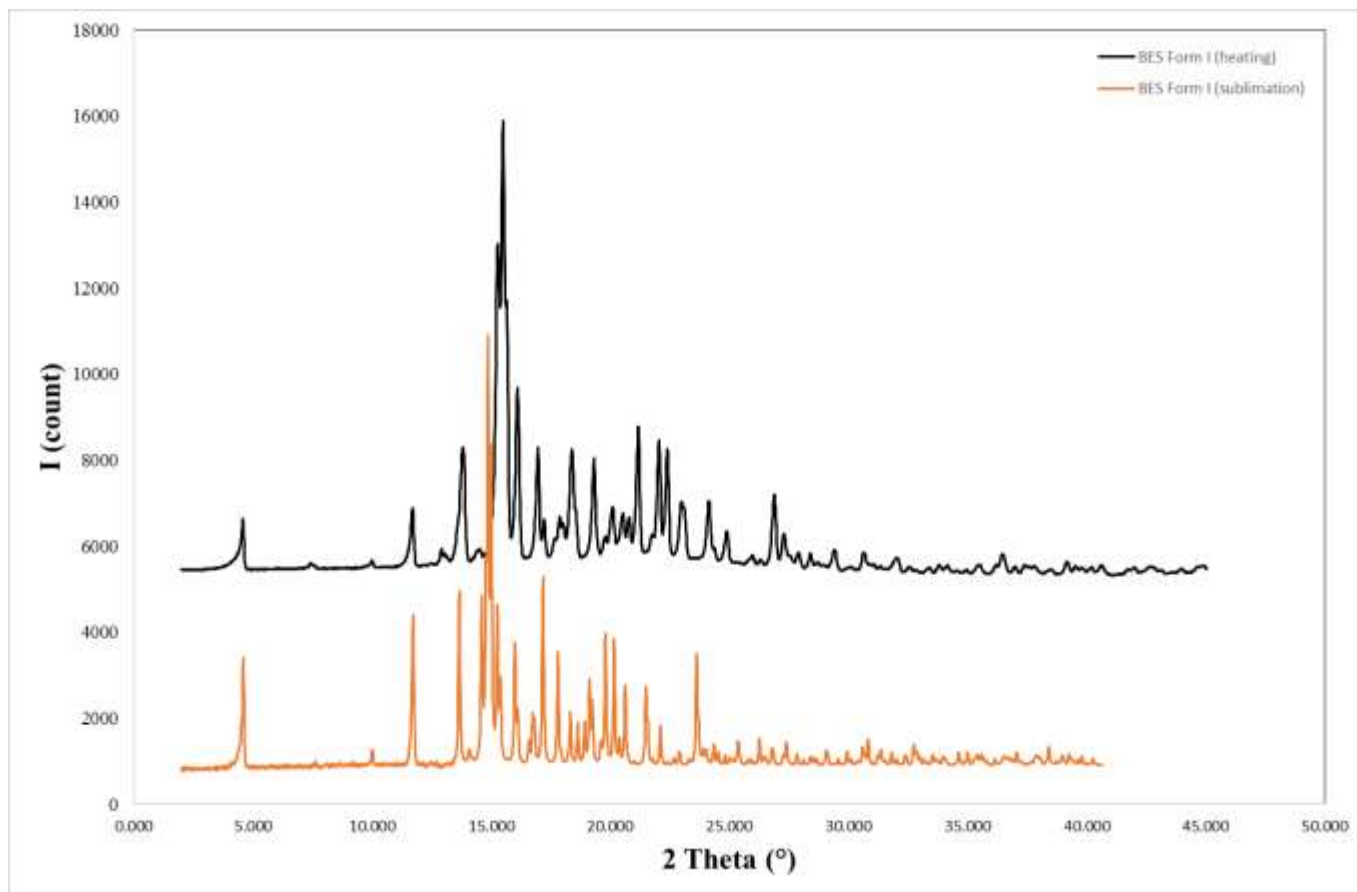
Figure S 6. PXRD data for BES Form I produced from heating experiments (black; method in experimental section of manuscript) and sublimation experiments (orange; method in A Section 1.4).

Section 4   Thermal Analysis

4.1. Thermal Analysis of BES·0.5H$_2$O kept in P$_2$O$_5$ Desiccator.
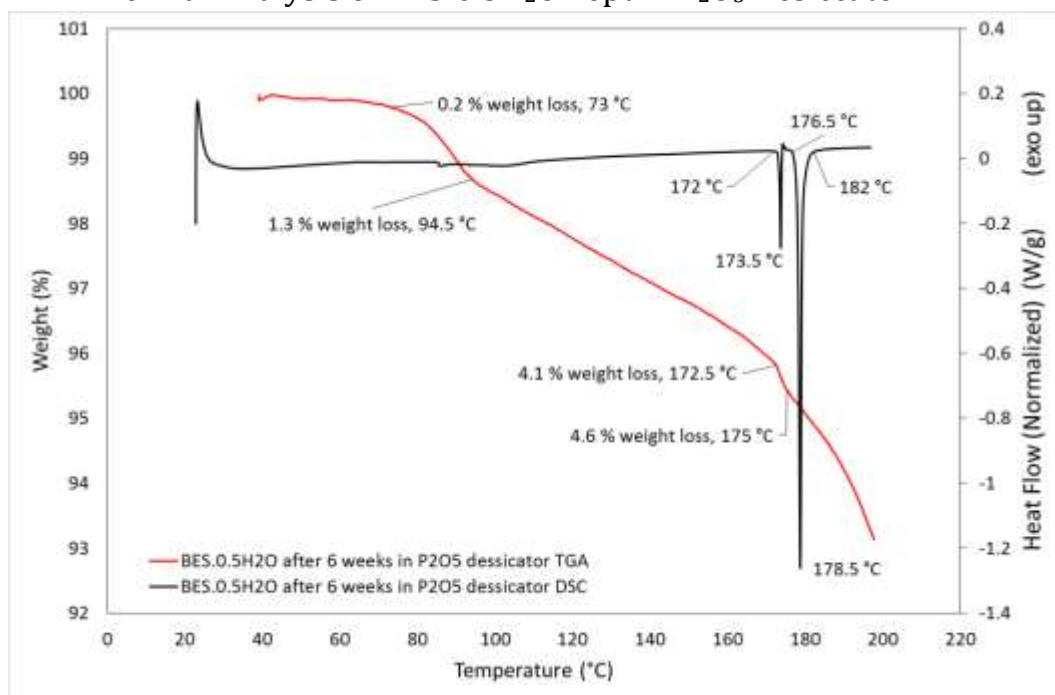
Figure S 7. DSC and TGA analysis of BES·0.5H$_2$O kept in P$_2$O$_5$ desiccator.

4.2. Thermal Analysis of BES
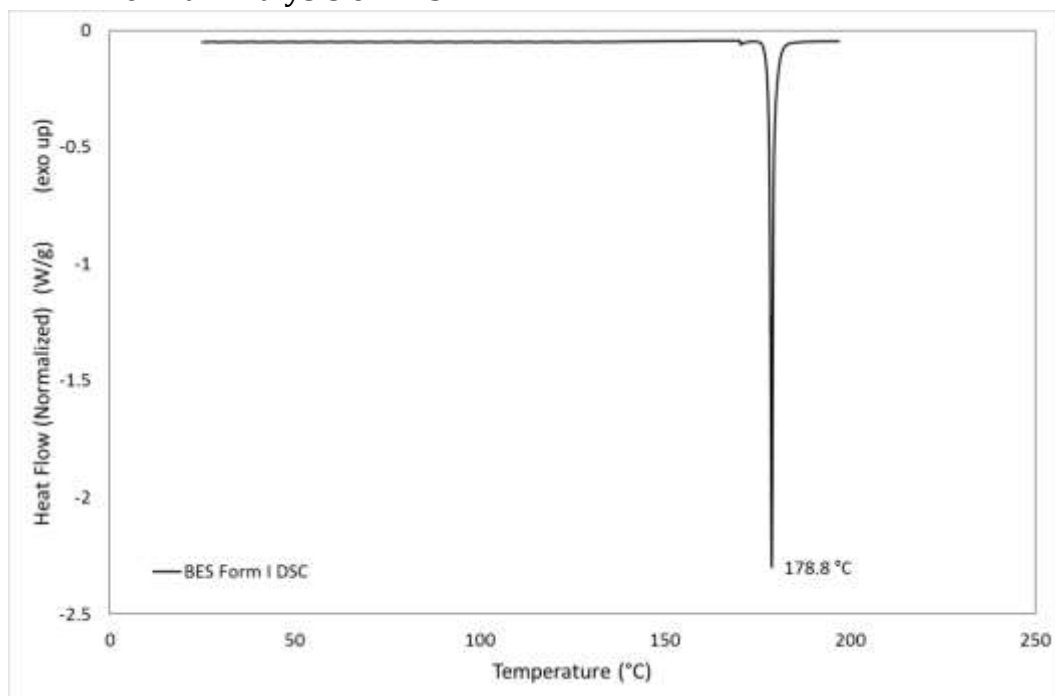
Figure S 8. DSC analysis of BES Form I
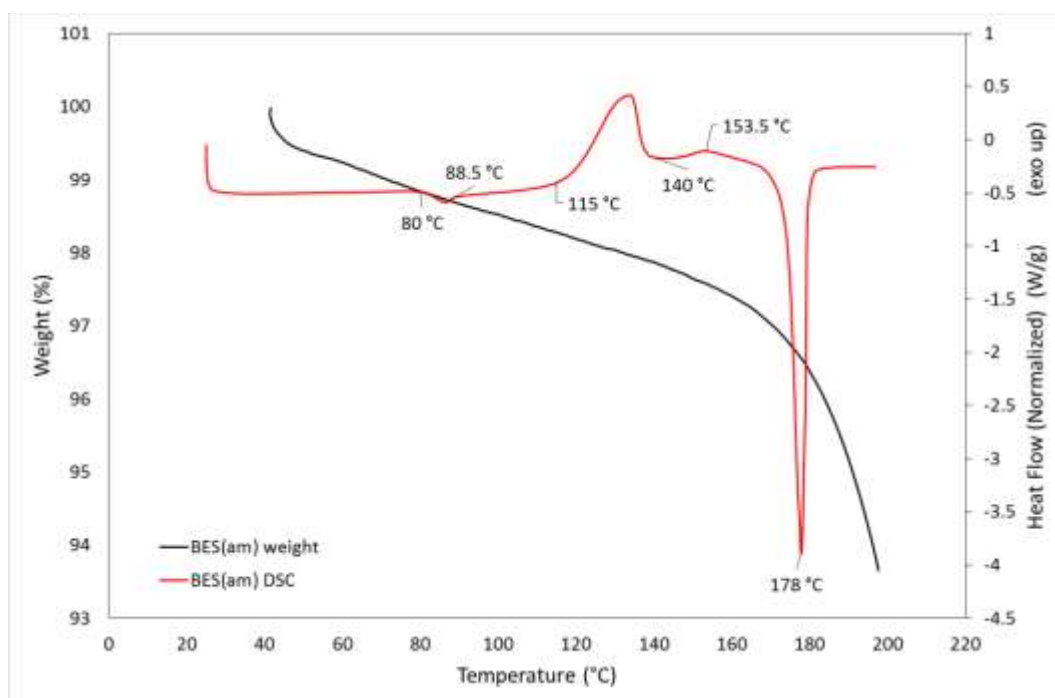
Figure S 9. DSC and TGA analysis of Form BES(am).

On heating BES(am) to 140 °C for 10 min on a hot stage microscope, crystallization into BES Form I took place, as confirmed by IR spectroscopy and PXRD. DSC analysis of BES(am) (Figure S 9) shows a small endothermic peak at 80 °C that indicates a glass transition. There is an exothermic peak at 115 °C and another exothermic peak just before the final melting endotherm at 178 °C. It is likely that this event at 115 °C is crystallization of an unknown form, which melts and recrystallizes to Form I at 153.5 °C.

11

4.3. Thermal analysis of solvates

(a)

(b)
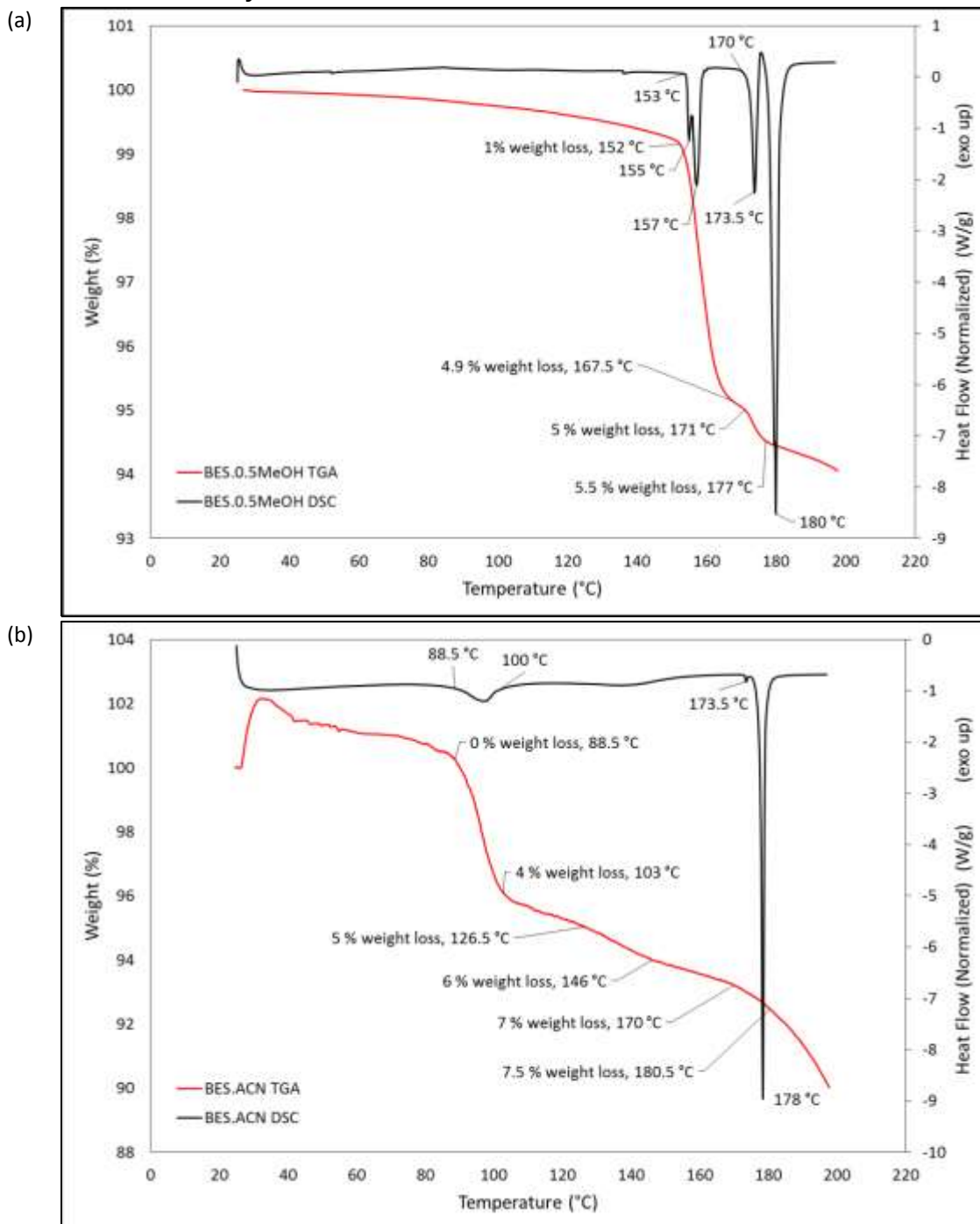
Figure S 10. Thermal data for BES·0.5MeOH and BES·ACN. (a) DSC (black) and TGA (red) of BES·0.5MeOH. (b) DSC (black) and TGA (red) of BES·ACN (noise present at the start of the DSC data collection is due to small sample mass).

DSC analysis of BES·0.5MeOH in single crystal form, heated at a rate of 10 °C min⁻¹ (Figure S 10a), shows three pre-melting endotherms. The first occurs at 155 °C as a shoulder on a peak at 157 °C and a third endotherm at 173.5 °C before the melting endotherm at 180 °C (Figure S 10a). The TGA analysis shows the first two endotherms correspond to 4.9% weight loss and the third corresponds to the complete loss of methanol leading to the overall stoichiometric weight loss of 5.5% (Figure S 10a). The melting endotherm occurs at a temperature slightly higher than the melting endotherm found by DSC for BES Form I (Figure S 8). The small difference in melting temperature could be due to a second anhydrous form of BES but it would require more investigation to confirm this. A small exothermic peak is noticeable overlapping with the end of the peak at 173 °C, which is also apparent in the hemihydrate sample dried with the desiccant in Figure S 7. This suggests a possible rearrangement to either the same or a different form.

12

The DSC analysis of BES·ACN shows three small pre-melting endotherms (Figure S 10b). The first and most prominent occurs between 88.5 and 100 °C, the second occurs between 125 and 152 °C, while the third is extremely small and occurs at 173.5 °C, just before the melting endotherm at 178 °C (Figure S 10b). The TGA analysis shows the first endothermic peak corresponds to a 4.5% weight loss and the second to a total 5% weight loss (Figure S 10b). The TGA isn't sufficiently sensitive to detect any change for the third endothermic peak. The weight loss appears to total 7.5% before melting at 178 °C. This is only approximately half the expected stoichiometric weight loss of 13% for complete desolvation, suggesting that complete solvent loss only occurs once BES·ACN melts. These values are not very accurate as the pan was not stable at the start of the experiment (as indicated by the "increase" in mass). This was due to the small sample size available.

B) Computational

Section 1   Conformational analysis

Two separate relaxed torsion angle scans were carried out on 17-β-estradiol, at the PBE0/6-31G(d,p) level of theory in GAUSSIAN (Figure S 11).
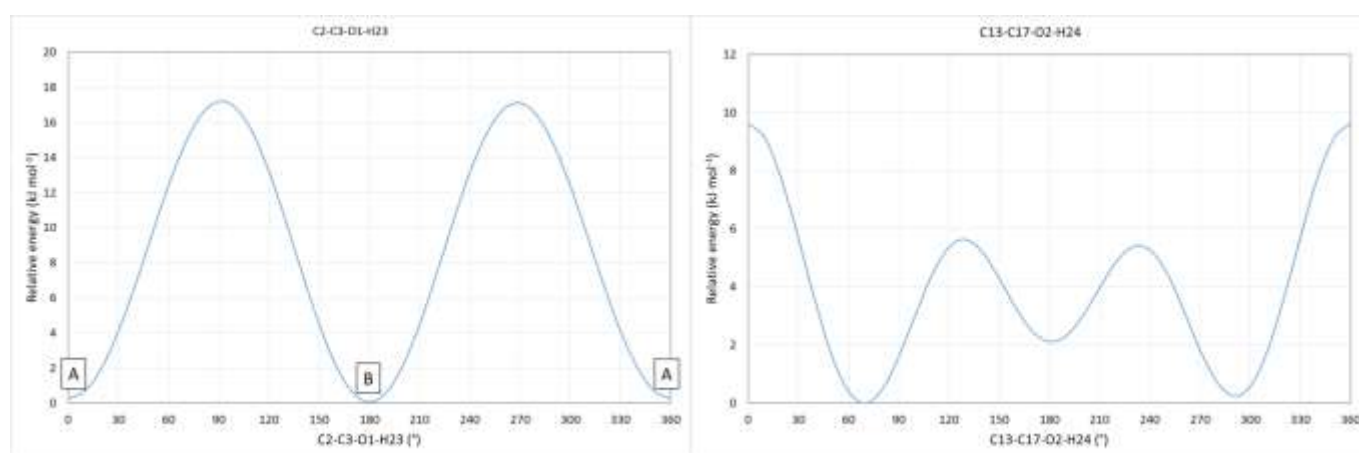
Figure S 11. Results of the relaxed torsion angle scans of 17-β-estradiol. (left) scan about C2-C3-O1-H23 and (right) scan about C13-C7-O2-H24 at the PBE0/6-31G(d,p) level of theory.

Figure S 11a showed that C2-C3-O1-H23 was more stable when approximately coplanar with the phenyl ring, and due to there being no ortho groups it is approximately equi-energetic at either position. In contrast, the C13-C17-O2-H24 angle shows three minima, with the configurations where O2-H24 is out of the plane of the 5-membered ring being more stable. The conformations are illustrated in Figure S 12.

B – C4-C3-O1-H23 = 180° (≡ C2-C3-O1-H23=0 on Figure S 11)

A – C4-C3-O1-H23 = 0° (≡ C2-C3-O1-H23=180 on Figure S 11)

C13-C17-O2-H24 = 70°

C13-C17-O2-H24 = 180°

C13-C17-O2-H24 = 290°
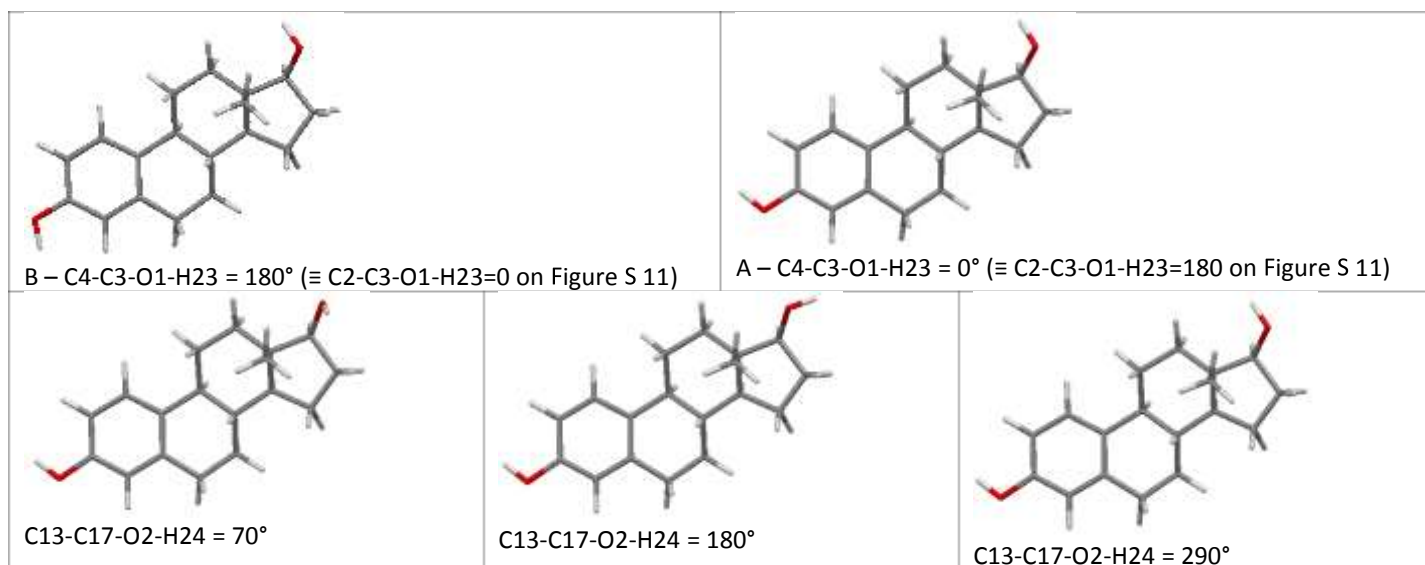
Figure S 12. Diagrams showing the low energy conformations identified in the torsion angle scans in Figure S 11.

13

Section 2 Computational Model Selection

2.1. Reproduction of Experimental BES·0.5H$_2$O and 17-α-estradiol

In order to ensure the computational modelling method is adequate to reproduce experimental structures, CrystalOptimizer[1] minimizations were carried out on BES·0.5H$_2$0, (refcode ESTDOL10) and 17-α-estradiol (refcode ESTTRD) taken from the CSD.[2] The PBE0/6-31G(d,p) method was used to obtain the molecular charge density and to calculate ΔE_{intra}, and repulsion-dispersion intermolecular energy terms were taken from the FIT empirical potential.[3] The torsions and C-O-H angles allowed to be flexible during the calculations are illustrated in Figure S 13
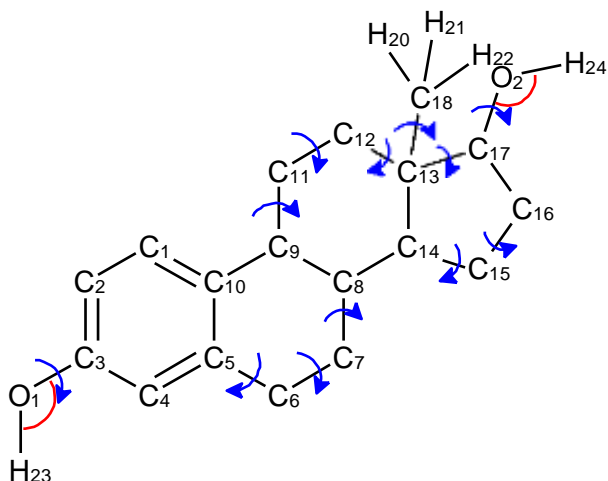
Figure S 13. Independent degrees of freedom refined in CrystalOptimizer for 17-(α/β)-estradiol

The results of the CrystalOptimizer minimizations including initial and final lattice energy ($E_{latt} = U_{inter} + \Delta E_{intra}$), initial and final cell constants and RMSD$_{30}$ overlay (calculated using the Crystal Packing Similarity feature in *Mercury*) of the experimental and optimized structures are found in Table S 5. Figure S 14 shows the overlay of experimental and optimized molecular conformations. These results were considered adequate.

Table S 5. Comparison of experimental and structures optimized with CrystalOptimizer. RMSD$_{30}$ is calculated with 40% distance and angle tolerances.

Structure		Lattice Energy (kJ mol^{-1})	A (Å)	B (Å)	c (Å)	α (°)	β (°)	γ (°)	RMSD$_{30}$ (Å)
BES·0.5H$_2$O (ESTDOL10)	Initial	-330.415	11.8265	19.7539	6.7272	90	90	90	0.290
	Final	-343.456	11.8643	19.0762	6.9247	90	90	90	
17 α-estradiol (ESTTRD)	Initial	-304.965	9.0038	23.4705	7.1388	90	99.8722	90	0.148
	Final	-320.904	9.2020	23.5294	7.2515	90	99.7199	90	
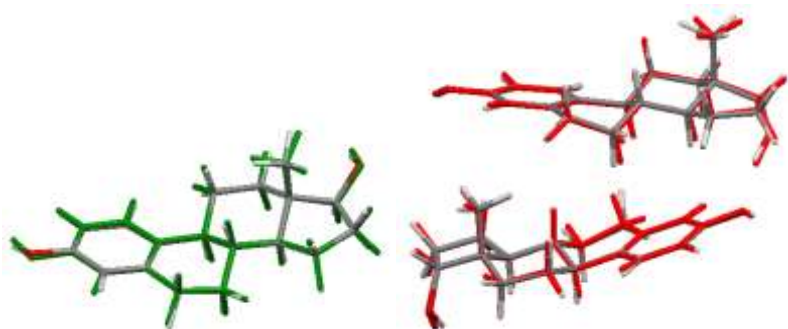
Figure S 14. Overlay of the estradiol molecules of the experimental and optimized crystal structures of (left) BES in the hemihydrate (ESTDOL10) with experimental structure coloured by element and optimized structure in green (RMSD$_1$=0.057 Å) and (right) 17-α-estradiol (ESTTRD) with experimental structure coloured by element and optimized structure coloured in red (RMSD$_2$=0.053 Å).

Section 3   Search methodology

3.1.   LAM generation for CrystalPredictor

CrystalPredictor2 uses a database of Local Approximate Models (LAMs) to describe the conformational energy (ΔE_{intra}) and charge density (distributed multipoles) of the flexible molecule as structures are minimized within the search algorithm. LAMs were generated using the PBE0 method in GAUSSIAN and the 6-31G(d,p) basis set, within the ranges described in Table S 6. Since each LAM is valid up to 50% of the step size in any degree of freedom, this covered all areas where the intramolecular energy of the molecule was less than ~10 kJ mol^{-1} above the global minimum (Figure S 11).

Table S 6. Boundaries of the LAM calculations for BES.

Region A			
Angle	lowest LAM point	highest LAM point	step size
C13_C17_O2_H24	10°	350°	20°
C2_C3_O1_H23	-40°	40°	20°
Region B			
Angle	lowest LAM point	highest LAM point	step size
C13_C17_O2_H24	10°	350°	20°
C2_C3_O1_H23	140°	40°	220°

3.2.   The CrystalPredictor search

The searches were carried out only in Z'=2, since large chiral molecules have a tendency to crystallize in Z'=2 structures. Only the most common chiral space groups ($P1$, $P2_1$, $P2_12_12$, $P2_12_12_1$, $C2$, $C222_1$, $P4_1$, $P4_3$, $P4_12_12$, $P4_32_12$, $P3_1$, $P3_2$, $R3$, $P3_121$, $P3_221$, $P3_221$, $P6_1$, $P6_3$, $P2_13$ and $P222_1$) were included. Each search generated 1,000,000 crystal structures, and minimized them with appropriate points from the LAM for estimating the conformational energy ΔE_{intra} and using the point charges and the FIT repulsion-dispersion potential for the intermolecular energy.

3.3.   CrystalOptimizer refinement

All structures within 15 kJ mol^{-1} of the lowest energy structure were reminimized with CrystalOptimizer, considering all of the angles marked in Figure S 13 as independent degrees of freedom. The torsion angles were C4-C3-O1-H23, C13-C17-O2-H24, C12-C13-C18-H20, C4-C5-C6-C7, C5-C6-C7-C8, C9-C8-C7-C6, C16-C15-C14-C8, H17-C16-C15-C14, O2-C17-C13-C12, C17-C13-C12-C11, C13-C12-C11-C9 and C12-C11-C9-C8 and the bond angles were C3-O1-H23 and C17-O2-H24. Both the intramolecular energy penalty (ΔE_{intra}) and the charge density for the distributed multipole analysis were calculated in GAUSSIAN at the PBE0 level of theory with the 6-31G(d,p) basis set. The FIT potential (with Coombes' variation for polar hydrogen atoms) was used to model the repulsion-dispersion contribution to the lattice energy. DMACRYS was used to minimize the lattice energy (U_{latt}). The total lattice energy ($E_{tot} = U_{latt} + \Delta E_{intra}$) was minimized with respect to all independent degrees of freedom.

3.4.   Crystal Structure Prediction summary

The full Crystal Structure Prediction summary of 17-β-estradiol with structures classified by space group is given in Figure S 15. The crystal energy landscape (the set of low energy structures that are potential observed polymorphs) is given in Figure S 16, with each structure categorized by hydrogen bonding motif and local packing.
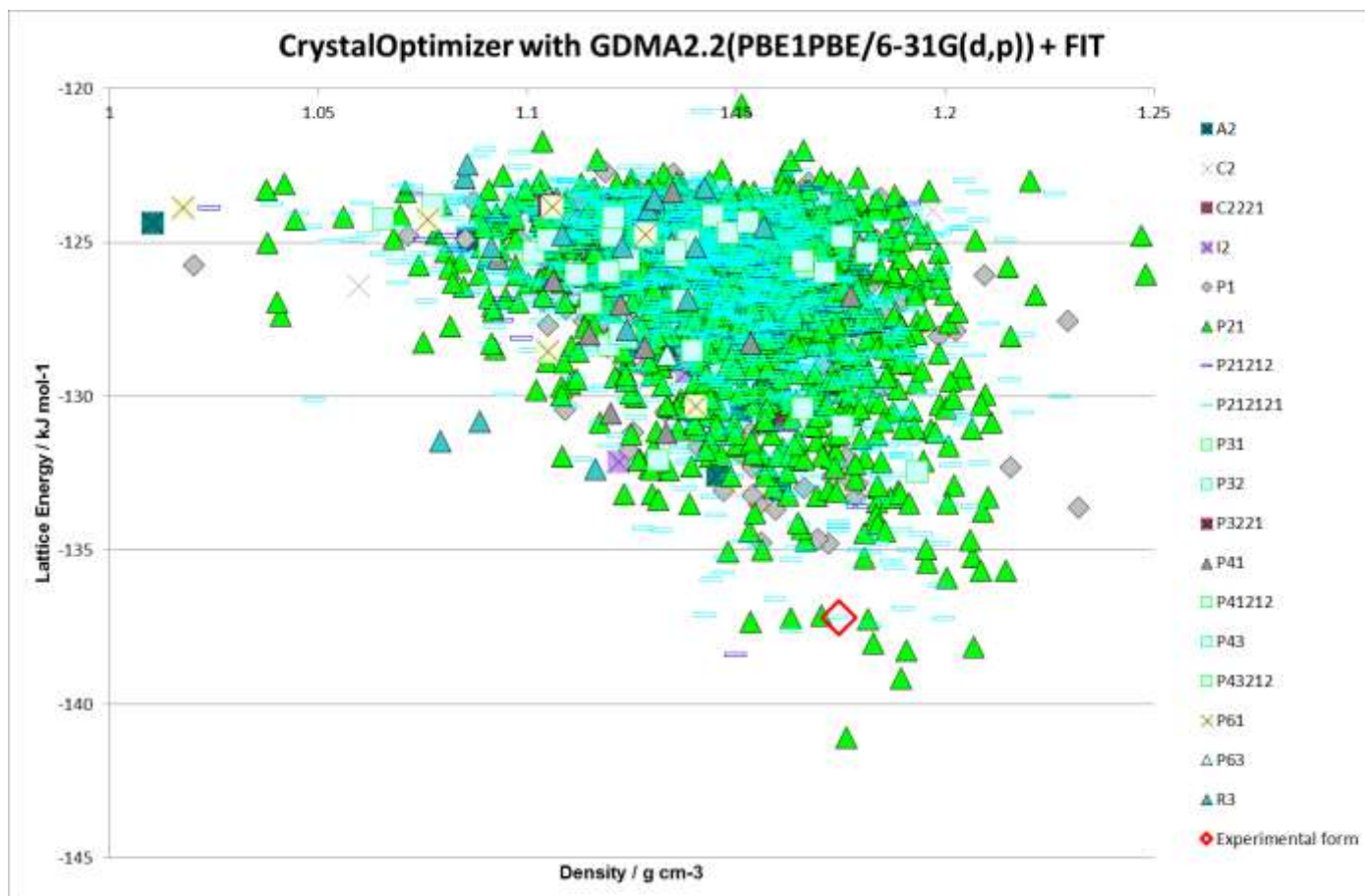
Figure S 15. Full crystal energy landscape of 17-β-estradiol. Each structure represents a lattice energy minimum, and is classified by space group.

3.5. Energetic comparisons of solvate structures

Each of the fully characterized solvate structures was minimized within the same computational model as described in Section 3.3 above, including appropriate independent degrees of freedom for the solvent molecule (H-C-C-N torsion and H-C-N bond angle for acetonitrile; Cl-C-C-Cl torsion for ethylene dichloride; H-C-O-H torsion angle for methanol; H-O-H bond angle for water). Those solvents that had crystal structures on the CSD were also minimized with the same independent degrees of freedom as selected for the solvate minimization.

16

Table S 7. Summary of calculations to ascertain solvent stabilization energy of solvates where solvate and solvent crystal structures available.

Solvate	Stoichiometry	Solvate energy* /kJ mol^{-1}	Anhydrous /kJ mol^{-1}	Solvent	Solvent energy /kJ mol^{-1}	Stabilization energy / kJ mol^{-1}	RMSD$_{15}$[†] / Å
Acetonitrile	BES·ACN	-185.943	-137.19	acetonitrile alpha (QQQCIV05)	-39.444	-9.30946	0.265
Acetonitrile	BES·ACN	-184.943	-137.19	acetonitrile beta (QQQCIV04)	-40.1517	-7.60174	0.265
Ethylene dichloride	BES·EDC	-173.957	-137.19	ethylene dichloride (DCLETH02)	-48.5493	11.78265	0.767
Methanol	BES$_2$·MeOH	-336.374	-137.19	methanol alpha (METHOL04)	-39.9384	-11.0279	0.139
Methanol	BES$_2$·MeOH	-335.374	-137.19	methanol beta (METHOL05)	-42.6766	-9.15875	0.139
Methanol	BES$_2$·MeOH	-334.374	-137.19	methanol gamma (METHOL03)	-38.5561	-10.719	0.139
Propanol	BES·PrOH	-204.229	-137.19	propanol	Not on CSD		0.22
Hemihydrate	BES$_2$·H$_2$O	-375.944	-137.19	ice II	-51.8174	-24.8735	0.259
Hemihydrate	BES$_2$·H$_2$O	-375.944	-137.19	ice IX	-51.2707	-25.1469	0.259
Hemihydrate	BES$_2$·H$_2$O	-375.944	-137.19	ice VIII	-54.2094	-23.6775	0.259
Hemihydrate	BES$_2$·H$_2$O	-375.944	-137.19	ice XIII	-51.3925	-25.0859	0.259
Hemihydrate	BES$_2$·H$_2$O	-375.944	-137.19	ice XI	-52.3825	-24.591	0.259
Hemihydrate	BES$_2$·H$_2$O	-375.944	-137.19	ice XIV	-51.6438	-24.9603	0.259
Hemihydrate	BES$_2$·H$_2$O	-375.944	-137.19	ice XV	-51.9016	-24.8314	0.259

*The solvate energy is given here per unit cell, the solvent energy is given per mole of solvent molecules and the stabilization energy is given per molecule of BES relative to BES Form I.

[†]The RMSD$_{15}$ is for a coordination shell of 15 molecules (i.e. < 15 molecules of BES), and compares the CrystalOptimizer minimized solvate structure with the experimental solvate structure.

The EDC solvate crystal structure obtained from incomplete SCXRD data had a poor RMSD$_{15}$ (only 3 molecules matched with the default settings) when optimized with a model that has proved adequate for the other experimental structures. This confirmed that the structural model was inadequate.

3.6. Motif analysis
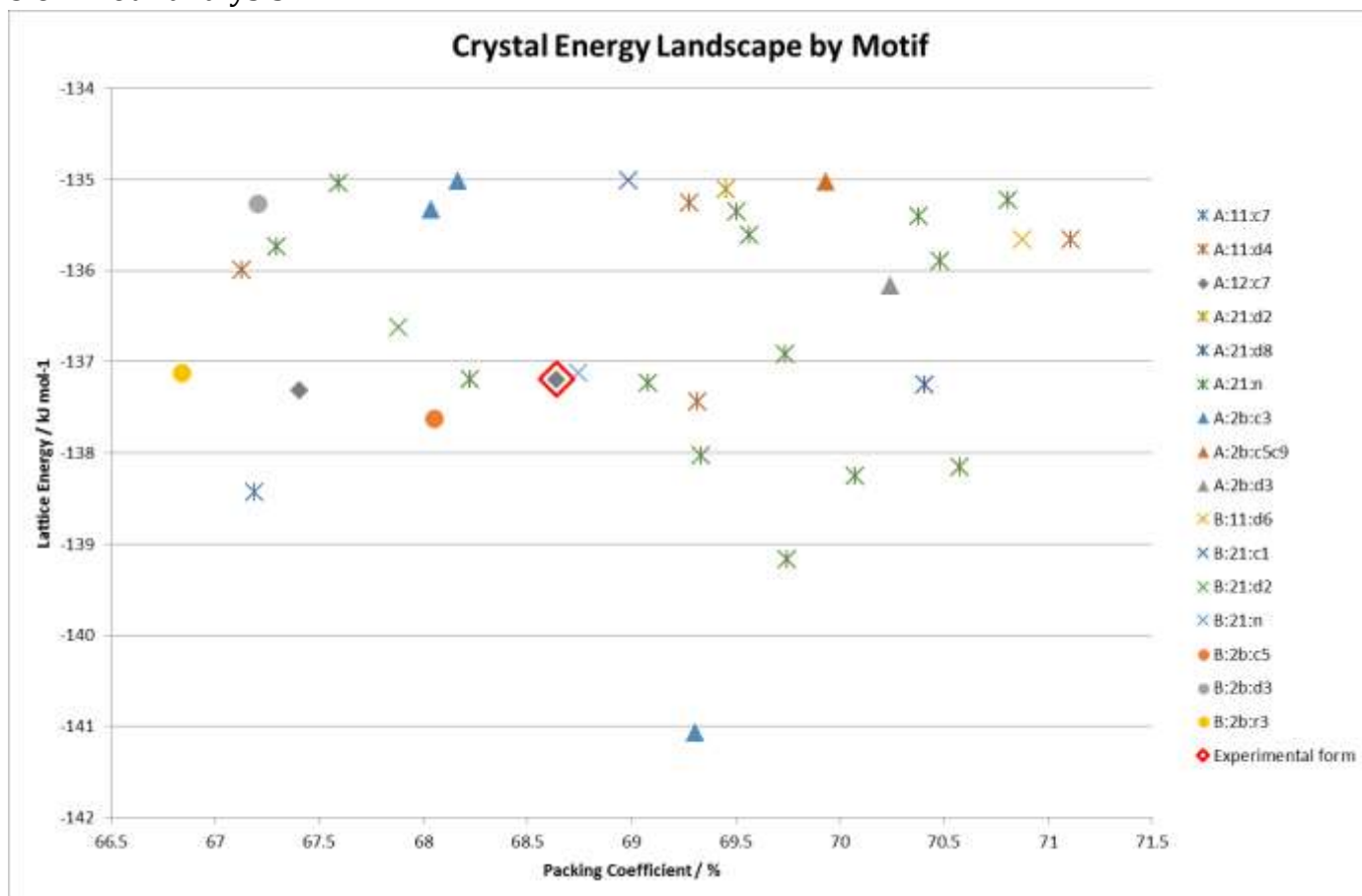
Figure S 16. Summary of the CSP study of BES. Each point corresponds to a structure which is a lattice energy minimum, calculated with the Ψ_{mol} method with intramolecular energy and charge density evaluated at the PBE0/6-31G(d,p) level and the FIT repulsion-dispersion model being used for the other terms. The structures have been categorized by motif X:nm:al where X=A or B denotes the O1H23 proton conformation; nm denotes the Chain 1 through-molecule hydrogen bonding type, with n denoting whether 1 or 2 molecules (of the Z'=2 molecules in the structure) are involved in through molecule hydrogen bonding and m denoting whether O1, O2 or both are acting as hydrogen bond donor; al denotes the Chain 2 hydroxyl-only hydrogen bonding type, n denotes that this is not present, c is that it is a chain, d a discrete interaction and r that it is a ring, the number l describes the order of the donor atoms along the hydroxyl only hydrogen bond motif as defined in Figure S 17.

The lowest energy structures (below -135 kJ mol⁻¹) on Figure S 15 were inspected and classified by their packing motifs, using Mercury. There were two common types of interaction, the through-molecule Chain 1 interaction and the hydroxyl-only Chain 2 interaction, pictured in Figure S 17. The through-molecule Chain 1 interaction can have O1-H23 or O2-H24 as the donor and O1 or O2 as the acceptor in the hydrogen bonds, although the most common is O1-H23···O2. A through-molecule interaction was seen for at least one symmetry independent molecule in all search-generated crystal structures. The structures were classified by whether one or both molecules had the through-molecule hydrogen bonded chain, and whether O1, O2 or both were the donor atom(s).

The hydroxyl-only interaction (Chain 2; Figure S 17) displays much more variety. It can vary the order of the groups, and can exhibit a continuous chain, discrete interaction (terminating after 3 or fewer hydrogen bonds) or a ring (in 1 case). Quite a few structures do not show this interaction at all (42%). The observed combinations are tabulated within Figure S 17.

18

Chain 1 "through-molecule"
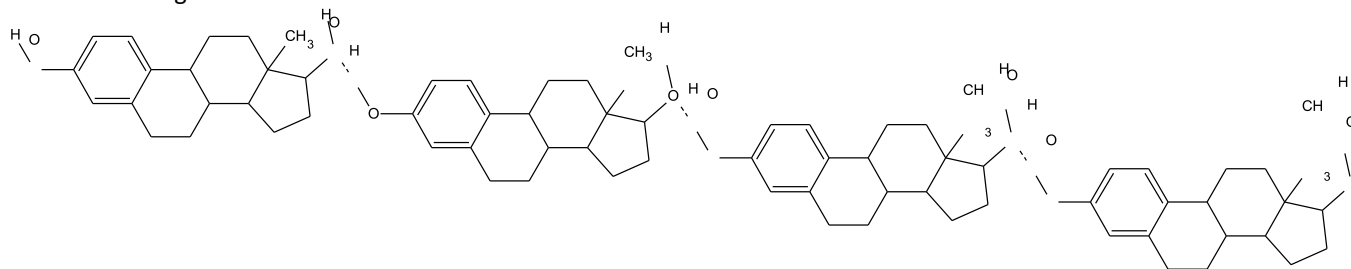
Donor/acceptor combination	Label	
O1 donor on 1 chain	11	
O1 donor on each of two chains	21	BES·ACN is 11, but only Z'=1
O1 donor with both molecules in one chain	21	
O2 donor on 1 chain	12	BES Form I is 12 BES·EDC is 12, but only Z'=1. BES·0.5H$_2$O is 12, but only Z'=1 BES·PrOH is 12, but only Z'=1
O1 donor on one chain and O2 donor on other chain	2b	BES·0.5MeOH is 2b
O1 donor and O2-donor in same chain	2b	
Discrete interaction through 3 molecules O2-H24···O3-M-O4-H48···O2	11	

Chain 2 "hydroxyl-only"
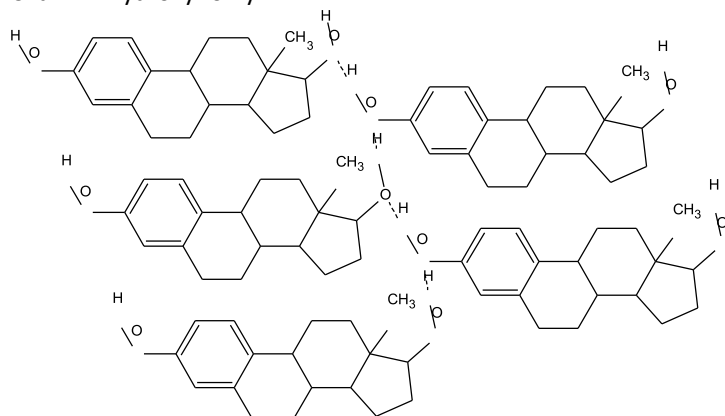
Repeat unit	Chain label	Discrete label	Ring label	Experimental observations
O1-H23···O2	c1	(d1)		BES·PrOH has O2-H24···O1-H23···S chains BES·0.5H$_2$O has O2-H24···O1-H23···S chains BES·ACN has O1-H23···O2-H24···S discrete interactions, as no hydrogen bond donor on solvent BES·EDC has O1-H23···O2-H24···S also has discrete interactions
O1-H23···O2-H24···O3-H47···O4-H48		d2		
O1-H23···O2-H24···O4-H48···O3-H47	c3	d3	r3	BES·0.5MeOH has O1-H23···O2-H24···O4-H48···O3-H47···S chain
O1-H23···O2-H24···O4-H48		d4		
O1-H23···O3-H47	c5			
O1-H23···O4-H48···O2-H24···O3-H47		d6		
O1-H23···O4-H48···O2-H24	c7			BES Form I has chain c7
O1-H23···O4-H48 ··O3-H47···O2-H24		d8		
O2-H24···O4	c9			

Figure S 17. Common hydrogen bonding motifs observed in low energy BES structures.

The experimentally observed crystal structures are dominated by Chain 1 interactions with O2 acting as the only hydrogen bond donor. In contrast, the crystal energy landscape has only two such structures on it, with all other

structures containing Chain 1 interactions with O 1 as the donor or both oxygen atoms as donors. The exception experimentally is the ACN solvate, where O1 is the donor in the through-molecule hydrogen bonded chains.

All experimental structures have the hydroxyl-only interaction, while 42% of the crystal energy landscape structures do not. In the case of the experimentally observed structures, the solvent molecule frequently participates in this chain (in the case of alcohols) or acts as the terminating group in the discrete interactions (in the case of solvent molecules with no hydrogen bond donor).

For both chain types, it is possible that alternatives with the hydrogen positions reversed appear somewhere on the crystal energy landscape. It may be that very closely matched alternatives would be removed by Clustering, but it may be that they are simply higher in energy and not in the set of low energy structures that have been analyzed.

3.7. Low Energy CSP-generated Structures.

Table S 8. Lowest 35 structures from the calculated lattice energy landscape. Structures are named by energy ranking after the initial CrystalPredictor clustering and preceded with the name of the search from which they were generated. Structures preceded with C were generated in search A. The structure files in .res format are available from the authors on request.

Label	ΔE_{intra} /kJmol^{-1}	Space Group	Z'	Z	a /Å	b /Å	c /Å	α /°	β /°	γ /°	Density /g cm^{-3}	Packing Coefficient	Intermolecular Lattice Energy /kJ mol^{-1}	Repulsion Dispersion Energy /kJ mol^{-1}	Lattice Energy /kJ mol^{-1}	Motif
C958	4.45	$P2_1$	2	4	9.5281	23.551	7.3867	90	111.888	90	1.1763	69.31	-145.52	-202.53	-141.07	A:2b:c3
A3174	0.976	$P2_1$	2	4	8.1265	9.3859	21.5384	90	67.801	90	1.1894	69.74	-140.14	-191.92	-139.164	A:21:n
C3583	2.5	$P2_12_12$	2	8	11.7988	37.1792	7.1735	90	90	90	1.1499	67.19	-140.93	-177.28	-138.43	A:11:c7
C374	2.393	$P2_1$	2	4	7.8819	21.5494	10.5052	90	121.616	90	1.1907	70.07	-140.64	-199.90	-138.247	A:21:n
C390	10.562	$P2_1$	1	2	6.1071	19.7431	6.4094	90	104.078	90	1.2068	70.57	-148.71	-193.46	-138.148	A:21:n
A136	2.329	$P2_1$	2	4	11.4516	8.0816	18.8495	90	61.261	90	1.1828	69.33	-140.35	-191.77	-138.021	A:21:n
D2	1.552	$P1$	2	2	7.3138	9.5352	12.1877	95.868	82.609	70.7	1.151	67.52	-139.42	-193.29	-137.868	A:2b:c3
B2208	2.742	$P2_12_12_1$	2	8	11.1826	7.4588	37.2916	90	90	90	1.1633	68.05	-140.37	-185.33	-137.628	B:2b:c5
A104	3.014	$P2_12_12_1$	2	8	28.2281	13.1022	8.2734	90	90	90	1.1825	69.31	-140.45	-197.38	-137.436	A:11:d4
A122	4.145	$P2_1$	2	4	20.1294	6.5489	11.9099	90	87.426	90	1.1535	67.40	-141.46	-174.22	-137.315	A:12:c7
C3274	3.606	$P2_12_12_1$	2	8	7.6322	17.5309	22.54	90	90	90	1.1998	70.41	-140.85	-208.38	-137.244	A:21:d8
C161	5.924	$P2_1$	2	4	6.8934	11.3044	20.8254	90	70.666	90	1.1815	69.08	-143.15	-186.5	-137.226	A:21:n
C2621	1.398	$P2_1$	2	4	10.4434	20.9755	7.4819	90	71.641	90	1.1631	68.22	-138.59	-189.25	-137.192	A:21:n
C252	4.31	$P2_12_12_1$	2	8	11.7383	7.1306	36.8083	90	90	90	1.1745	68.64	-141.5	-186.23	-137.19	A:12:c7
B33	2.542	$P2_12_12_1$	2	8	26.0154	12.2574	9.9298	90	90	90	1.1427	66.84	-139.67	-176.45	-137.128	B:2b:r3
B1319	0.779	$P2_1$	2	4	7.6227	16.3101	12.4337	90	89.994	90	1.1704	68.74	-137.9	-191.59	-137.121	B:21:n
A45	3.26	$P2_12_12_1$	2	8	11.308	7.4621	36.0296	90	90	90	1.1902	69.74	-140.17	-194.1	-136.91	A:21:n
B12	1.416	$P2_12_12_1$	2	8	9.795	12.3616	25.7735	90	90	90	1.1595	67.88	-138.03	-189.27	-136.614	B:21:d2
A355	5.567	$P2_12_12_1$	2	8	22.0152	10.3419	13.2548	90	90	90	1.199	70.24	-141.73	-199.31	-136.163	A:2b:d3
A2029	0.566	$P2_12_12_1$	2	8	21.6451	8.1019	18.0308	90	90	90	1.1443	67.13	-136.55	-188.48	-135.984	A:11:d4
C3159	5.423	$P2_1$	2	4	11.0821	21.2585	7.618	90	57.113	90	1.2005	70.48	-141.31	-199.2	-135.887	A:21:n
C2059	1.422	$P2_12_12_1$	2	8	10.4123	21.045	14.3967	90	90	90	1.147	67.29	-137.16	-183.79	-135.738	A:21:n
B14	2.581	$P2_1$	2	4	15.2574	14.0213	7.02	90	85.469	90	1.2085	70.87	-138.24	-212.14	-135.659	B:11:d6
C437	5.688	$P2_1$	2	4	7.5701	18.9055	10.4118	90	91.343	90	1.2145	71.11	-141.34	-208.55	-135.652	A:11:d4
C119	5.129	$P2_12_12_1$	2	8	19.5316	6.9255	22.5142	90	90	90	1.1881	69.56	-140.73	-191.61	-135.601	A:21:n
C131	4.102	$P2_1$	2	4	9.3227	22.3996	7.7305	90	69.61	90	1.1956	70.38	-139.5	-203.07	-135.398	A:21:n
A489	4.119	$P2_12_12_1$	2	8	7.9817	21.7019	17.5944	90	90	90	1.1873	69.50	-139.47	-199.47	-135.351	A:21:n
C364	6.42	$P2_12_12_1$	2	8	13.8418	9.5362	23.5672	90	90	90	1.1632	68.03	-141.75	-194.9	-135.33	A:2b:c3
B41	1.208	$P2_12_12_1$	2	8	12.2862	34.4771	7.445	90	90	90	1.1474	67.21	-136.47	-190.96	-135.262	B:2b:d3
A310	2.935	$P2_1$	2	4	13.0646	8.2379	14.8903	90	72.993	90	1.1806	69.28	-138.19	-195.26	-135.255	A:11:d4
A60	1.348	$P2_1$	2	4	9.1282	12.4523	13.196	90	88.581	90	1.2066	70.81	-136.57	-210.58	-135.222	A:21:n
C2642	7.117	$P2_12_12_1$	2	8	11.6826	22.8558	11.4637	90	90	90	1.1821	69.45	-142.22	-194.83	-135.103	A:21:d2
C305	1.425	$P2_1$	2	4	8.134	21.5724	8.9807	90	89.91	90	1.1481	67.59	-136.46	-174.19	-135.035	A:21:n
C352	4.009	$P2_12_12_1$	2	8	13.059	39.411	5.9028	90	90	90	1.1911	69.93	-139.03	-204.35	-135.021	A:2b:c5c9
A36	4.075	$P2_12_12_1$	2	8	10.1996	12.8742	23.6121	90	90	90	1.167	68.17	-139.09	-193.7	-135.015	A:2b:c3
B3039	7.336	$P2_12_12_1$	2	8	9.9202	25.3218	12.2146	90	90	90	1.1793	68.98	-142.34	-200.55	-135.004	B:21:c1

References

1.	A. V. Kazantsev, P. G. Karamertzanis, C. S. Adjiman and C. C. Pantelides, in *Molecular System Engineering*, eds. C. S. Adjiman and A. Galindo, WILEY-VCH Verlag GmbH & Co., Weinheim, 2010, vol. 6, pp. 1-42.
2.	C. R. Groom, I. J. Bruno, M. P. Lightfoot and S. C. Ward, Acta Crystallographica Section B-Structural Science Crystal Engineering and Materials, 2016, **72**, 171-179.
3.	D. S. Coombes, S. L. Price, D. J. Willock and M. Leslie, *Journal of Physical Chemistry*, 1996, **100**, 7352-7360.